Chemical Engineering Science: X 11 (2021) 100100

Contents lists available at ScienceDirect

Chemical Engineering Science: X

journal homepage: www.elsevier.com/locate/cesx

Experimental and numerical insights into heterogeneous liquid-solid behaviour in drinking water softening reactors

T.M.J. Nijssen [a,1], O.J.I. Kramer [b,c,d,e,f,1], P.J. de Moel [d,g], J. Rahman [f], J.P. Kroon [a], P. Berhanu [f], E.S. Boek [f], K.A. Buist [a,*], J.P. van der Hoek [b,d], J.T. Padding [c,*], J.A.M. Kuipers [a]

[a] Eindhoven University of Technology, Department of Chemical Engineering & Chemistry, Multiphase Reactors Group, PO Box 513, Eindhoven 5600 MB, the Netherlands
[b] Delft University of Technology, Faculty of Civil Engineering and Geosciences, Department of Water Management, PO Box 5048, 2600 GA Delft, the Netherlands
[c] Delft University of Technology, Faculty of Mechanical, Maritime and Materials Engineering, Department of Process and Energy, Leeghwaterstraat 39, 2628 CB Delft, the Netherlands
[d] Waternet, PO Box 94370, 1090 GJ Amsterdam, the Netherlands
[e] HU University of Applied Sciences Utrecht, Institute for Life Science and Chemistry, PO Box 12011, 3501 AA Utrecht, the Netherlands
[f] Queen Mary University of London, Division of Chemical Engineering, School of Engineering and Materials Science, Mile End Road, London E1 4NS, United Kingdom
[g] Omnisys, Eiberlaan 23, 3871 TG Hoevelaken, the Netherlands

ARTICLE INFO

Article history:
Received 15 February 2021
Received in revised form 23 April 2021
Accepted 1 May 2021

Keywords:
Fluidisation
Unsteady behaviour
Drinking water treatment
Multiphase computational fluid dynamics
Reactor performance
Void fraction distribution

ABSTRACT

Liquid-solid fluidisation is frequently encountered in drinking water treatment processes, for instance in seeded crystallisation softening processes. For modest superficial fluid velocities, liquid–solid fluidisation systems are generally considered to be homogeneous, as reported in literature. However, during fluidisation experiments with calcite grains, open spaces of water can be observed between the fluidised particles, even at relatively low fluid velocities. Moreover, significant heterogeneous particle–fluid patterns are detected at higher fluid velocities. Such heterogeneous behaviour can beneficially or adversely affect the chemical crystallisation efficiency. To obtain information about voids in bulk regions, complementary Computational Fluid Dynamics - Discrete Element Method (CFD-DEM) simulations were performed and compared with the experimental results for validation. Simulations were performed using different water inlet velocities and fractionised calcite granules obtained from full-scale reactors. Here, the results are analysed using the bed height, voidage and pressure drop of the system. Furthermore, images of the experiments and simulations are visually compared for the formation of voids. The simulations showed distinct differences in void fraction in the cross-section of the column. It is shown that throughout the range of considered water velocities, heterogeneous behaviour exists and cannot be neglected. The heterogeneity and onset of fluidisation behaviour obtained from the simulations and experimental observations were compared and found to agree reasonably well.

1. Introduction

1.1. Liquid-solid fluidisation applied in drinking water softening processes

Water softening is an important process in water treatment (Crittenden et al., 2012). The removal of calcium carbonate has multiple benefits, for example to counteract limescale (Beeftink et al., 2021); (Kramer et al., 2020b). The softening process is frequently performed using liquid–solid fluidised (LSF) bed reactors (Fig. 1) (Graveland et al., 1983). In the Netherlands, more than 400 million m^3 water is softened annually in drinking water treatment plants employing fluidised bed pellet reactors (Hofman et al., 2007). By adding caustic soda, supersaturated conditions are created. Calcium carbonate crystallisation takes place on the surface of calcite grains, which then grow. Pellets are extracted from the reactor when a defined grain size threshold is exceeded. Larger particles will migrate to the lower region of the reactor bed and, depending on the flow conditions, a stratified bed with a certain particle size profile will evolve. In these softening reactors, sand is generally used as seeding material and calcite pellets are produced as a by-product (van Dijk and Wilms, 1991). To improve sustainability, pure calcite can be used as seeding material, while full-grown calcite pellets, extracted from the reactor, can be dried, grained and sieved and re-used as seeding material (Schetters et al., 2015).

* Corresponding authors.
E-mail addresses: t.m.j.nijssen@tue.nl (T.M.J. Nijssen), onno.kramer@waternet.nl (O.J.I. Kramer), k.a.buist@tue.nl (K.A. Buist), j.t.padding@tudelft.nl (J.T. Padding).

[1] Shared first authorship.

https://doi.org/10.1016/j.cesx.2021.100100
2590-1400/

Nomenclatures

Ar	Archimedes number [-]
C	Column length [m]
D	Inner column or cylinder vessel diameter [m]
d_p	Particle diameter [m]
e_p	Particle coefficient of restitution [-]
Fr	Froude number [-]
g	Gravitational acceleration [m/s^2]
L	Fluid bed height [m]
m_p	Total particle mass [kg]
$\Delta P/L$	Pressure drop/head loss [kPa/m]
ΔP_{max}	Total maximum differential pressure over the bed [kPa]
r	Radial coordinate [m]
St	Stokes number [-]
v_{mf}	Minimum fluidisation velocity [m/s]
v_s	Linear superficial velocity or empty tube fluidisation velocity [m/s]
v_t	Terminal settling velocity [m/s]
T	Temperature [°C]
V	Volume [m^3]
Y_p	Particle Young's modulus [MPa]
z	Axial coordinate [m]

Greek symbols

Δt	Time step [s]
Δx	Cell size [m]
ε	Voidage of the system [-]
$\widehat{\varepsilon}$	Voidage, integration variable [-]
η_f	Fluid dynamic viscosity [Pa•s]
μ_p	Particle coefficient of friction [-]
v_p	Particle Poisson ratio [-]
ρ_f	Fluid density [kg/m^3]
ρ_p	Particle density [kg/m^3]
σ_p	Particle diameter standard deviation [m]
σ_ε	Voidage standard deviation [-]
ϕ_m	Time-averaged vertical solid mass flux [kg/(m^{2}s)]

Abbreviations

ARE	average relative error
CCCP	calcium carbonate crystallisation potential
CDF	cumulative distribution function
CFD	computational fluid dynamics
DEM	discrete element method
GSF	gas–solid fluidisation
HU-ILC	University of Applied Sciences Utrecht, Institute for Life Science and Chemistry
LSF	liquid–solid fluidisation
PDF	probability density function
QMUL	Queen Mary University of London
SSA	specific surface area

Fig. 1. Full-scale pellet softening reactors located at Waternet (Amsterdam, the Netherlands). The unit consists of 12 Amsterdam reactors with reactor diameterD = 3.0 m (van der Veen and Graveland, 1988).

For optimal process conditions, *i.e.* fast calcium carbonate crystallisation (van Schagen, 2009), a large specific surface area (SSA), and therefore small particles, in the fluidised bed is required (Kramer et al., 2020b). Because of the importance of the grain size and subsequent stratification effects, the fluidisation behaviour of these LSF bed reactors must be studied closely. Due to the need to ensure a continuous production of reliable drinking water, experiments in this field are restricted to pilot-scale set-ups. Complementary to these experiments, numerical simulations are used as a reliable tool to gain insight into these processes. Such simulations offer a more detailed view of the fluidisation behaviour inside the reactor without the need for elaborate experimental methods.

1.2. Fluidisation quality

Homogeneous fluidisation can be defined as a fluidised state in which solid particles are uniformly dispersed throughout the fluid without observable bubbles (Yang, 2003). The average distance between particles remains relatively constant, such that there is a consistent distribution of neighbour particles around each given particle (Gibilaro, 2001). Mainly, no bubbles or voids are present in homogeneous fluidisation (Grace et al., 2020).

Heterogeneous fluidisation, in contrast, includes any state other than homogeneous. It can be chaotic or non-uniform, it can have bubbles or particles moving in bulk in different directions, and it can have particles moving randomly without maintaining a fixed distance to other particles. Both homogeneous and heterogeneous fluidisation are affected by increasing flow rate and varying particle properties. Fluidisation quality has been studied in great detail for gas–solid fluidisation (GSF) where bubbles play an important role. In LSF, bubbles or voids are pockets of fluid created during fluidisation. Some particles will get closer together to allow for large gaps with little or no particles. The presence of these gaps is one of the main indications of heterogeneous fluidisation (Geldart, 1973).

Homogeneous fluidisation for uniform particles was observed by Wilhelm and Kwauk (1948) who proposed a simplified classification and empirical criterion for the transition between a state of particulate or idealised fluidisation with complete homogeneity and a state of aggregative or heterogeneous fluidisation (Liu et al., 1996). Goossens (1998) proposed a relatively simple industrial tool to classify and predict the fluidisation behaviour of any given fluid-particle system, based upon the dimensionless Archimedes number $\mathrm{Ar} = g{d_p}^3 \rho_f \left|\rho_p/\rho_f - 1\right| / {\upsilon_f}^2$, where gravitational and inertial forces are considered, and taking into consideration a representative particle diameter and related shape factor.

It is widely accepted that fluidisation flow for GSF is heterogeneous or aggregative, while LSF is mainly homogeneous or particulate, implying that the particles are assumed to be uniformly

distributed (Ruckenstein, 1964); (Davidson et al., 1985); (Jamialahmadi and Miiller-Steinhagen, 1992); (Yang, 2003); (Crowe and Group, 2006); (Albright, 2009); (Wang et al., 2016); (Michaelide et al., 2017). This assumption has formed the basis of many publications. For example, Richardson and Zaki (1954) stated that measuring sedimentation would be similar to fluidisation due to the fact that in fluidisation the particles do not undergo any net movement and velocity is only due to the continuous upward movement of fluid, suggesting that the fluidisation reaches an equilibrium. Oke et al. (2015) assumed the Richardson-Zaki equation to be correct, implying that homogeneous flow dominates for their numerical calculations. This highlights the large influence that these older publications continue to have. According to Di Felice (1995), the main or prevalent regime is homogeneous in LSF, whereas GSF is described to have many regimes and transition states. Zheng et al. (1999) stated that the flow in a liquid–solid circulating fluidised bed has higher uniformity than is the case for a gas–solid bed and that only some non-uniformity can be seen, implying that the flow is mainly homogeneous. Liu et al. (2013) described LSF as pseudo-homogeneous for higher viscosity liquids. Tsuchiya et al. (1997) stated that LSF sometimes demonstrates heterogeneous behaviour, albeit mainly homogeneous. According to Batchelor (1988), the conditions for instability of LSF are more complicated compared to GSF. Batchelor described experiments trying to find relationships between flow rate and other variables and found that a non-uniform fluidised bed contains two dependent variables; the local mean particle velocity and the local particle concentration. Batchelor also showed that instability occurs when the particle Froude number $\mathrm{Fr} = v_s/\sqrt{gd_p}$ (ratio of inertial to gravity forces) exceeds a critical value (Wilhelm and Kwauk, 1948). A transition occurs from smooth homogeneous fluidisation to heterogeneous or aggregative (bubbling) fluidisation at a $\mathrm{Fr} \approx 1$. Fazle Hussain (1986) found that the instabilities of local turbulent flows cause the formation of vortices and coherent structures. Based on a stability map proposed by Gibilaro et al. (1986) and updated later (Gibilaro, 2001), the transition for LSF in ambient water from particulate to aggregate fluidisation depends on both the density and the size of the suspended particles; for a lower particle density, a larger size is necessary for a transition to occur.

While the majority of researchers have used optical methods to investigate LSF, a small number of computational studies is available too. For example, Ghatage et al. (2014) conducted an extensive literature review on the stability analysis of LSF and studied the transition from homogeneous to heterogeneous regimes with Computational Fluid Dynamics - Discrete Element Method (CFD-DEM) simulations and experiments. This study highlighted that the transition conditions for LSF could be obtained experimentally by observing the behaviour of the (classification) velocity of a single foreign particle at different superficial liquid velocities.

1.3. Full-scale experience and reactor performance

The fluidisation quality of softening processes at Waternet, the water utility of Amsterdam and surroundings, was observed visually during full-scale operational conditions and considered to be moderately heterogeneous. It is currently unknown to which extent such heterogeneous behaviour affects the chemical crystallisation efficiency, either negatively or positively, as there are many effects to consider. In addition, carryover at the reactor effluent was detected, a process which adversely affects the calcium carbonate crystallisation potential (CCCP), a quality performance index for the water softening process (Rietveld, 2005).

The cylindrical pellet softening reactor (*Amsterdam reactor*) (van der Veen and Graveland, 1988) is based on well-mixed water, caustic soda and particular material in the lowest region of the reactor (continuously ideally stirred-tank reactor principle) and a continuous flowing system of cylindrical geometry (plug flow reactor principle) in upward direction. The rate of crystallisation is strongly dependent on the rate of mass transfer of the reactants to the crystallisation surface. As a consequence, the degree of heterogeneity is also important since bubbles cause bypass and liquid backflow, typically detrimental to the conversion.

The main advantage of seeded crystallisation employed in this reactor is that $CaCO_3$ precipitates onto the surface of grains instead of creating spontaneous unwanted precipitation in the liquid (Burhenne et al., 2017). The SSA of the seeding material is an important parameter for the softening process, as it influences the calcium carbonate kinetics significantly (van Dijk and Wilms, 1991); (van Schagen, 2009). The chemical performance of the seeded crystallisation is based on the growth rate of the seeding calcite particles (Hu et al., 2017) and the growth rate of the seeding material particle depends on the mass transfer of the reactants to the surface of the pellet and the reaction of crystallisation (Tai et al., 2006).

The imposed SSA which is exposed for crystallisation varies through time and space. Larger open water spaces might increase the probability of spontaneous precipitation, while a heterogeneous flow regime could have a positive effect on the dispersion of chemical reactants in the water phase due to vigorous agitation of the particles in contact with the fluid. It is unclear how the crystallisation proceeds in the presence of unsteady local voids during fluidisation. These combined factors mean that it is difficult to predict the influence of heterogeneous fluidisation on the reactor performance a priori. For this reason, a scaled pilot experimental setup was designed to investigate the hydraulic behaviour of the pellet softening process, and a CFD-DEM model was developed to study the degree of unsteady liquid–solid behaviour in LSF systems.

1.4. Aims

The aim of the current work is to demonstrate the importance of heterogeneous behaviour in LSF beds with calcite pellets in water. To this end, the instability of the local voidage and the overall transport of particles are used as indicators. Numerical modelling is applied using a suitable CFD-DEM model, and results are compared with reliable expansion data obtained from experiments. Additionally, quasi 2D images of inhomogeneities in the expanded beds are presented, taken from experiments as well as simulations. Lastly, the CFD-DEM model is used to explore the three-dimensional flow phenomena inside the LSF bed.

2. Materials and methods

2.1. Simulations

The simulations in this work were conducted using the model described in detail by Nijssen et al. (2020). This model couples Computational Fluid Dynamics and the Discrete Element Method, allowing for the simultaneous description of the water phase and the suspended particles. This work employs the unresolved CFD-DEM methodology, which resolves the fluid flow at a length scale larger than the particles. This allows for the simulation of a large number of particles ($\lessapprox 10^6$), but requires interaction models to evaluate the force exerted by the fluid on the particles and vice versa. The model proposed by Nijssen *et al.* is especially suited for simulation of LSF beds as it includes closures for the drag and lift as well as virtual mass and Basset forces. The addition of the Basset force is a significant improvement of the classical drag-only CFD-DEM approach, which is better suited for gas–solid sys-

tems (Nijssen et al., 2020). For a complete description of the model, the reader is referred to the original work.

The parameters and settings used in the simulations are summarised in Table 1. The fluid properties are taken at 20 °C, the same temperature at which the experiments were conducted. The coefficients of friction and restitution were estimated based on the experiments using glass spheres as performed by Joseph and Hunt (2004) and the Stokes number $\mathrm{St} = d_p \rho_f v / \left(9\eta_f\right)$. Using the liquid velocity as the typical collision velocity, the Stokes number was found to lie in the range of 10–60. Typical values were chosen for the Young's modulus and Poisson ratio, as they have a negligible influence on the results (Blais and Bertrand, 2017).

2.2. Experimental set-up

Expansion experiments for several materials were carried out at three locations: in Waternet's Weesperkarspel drinking water pilot plant located in Amsterdam, the Netherlands (Fig. 2a); at the Institute for Life Science and Chemistry of University of Applied Sciences Utrecht (HU-ILC), the Netherlands (Fig. 2b); and at Queen Mary University of London (QMUL), United Kingdom (Fig. 2c). Information about the expansion columns, fluidisation expansion experiments and standard operating procedures can be found in the Supplementary Material (Section 2).

The set-up (Fig. 3) consisted of a 4 m transparent PVC pipe with an inner diameter of 57 mm. The expansion set-up has two main circuits in which water flows: the expansion circuit and the temperature conditioning circuit. In the expansion circuit, a pump takes water from a reservoir and feeds it to the expansion column with an adjustable water flow. The flow rate entering the system can be controlled by opening and closing a valve in combination with an installed flow meter. The pressure drop was measured with a differential pressure sensor. The temperature conditioning circuit was used to deliver a desired temperature to the expansion circuit to perform expansion experiments at different temperatures. The circuit consists of a pump that feeds water into an integrated heating or cooling unit. Particles are fluidised in a cylindrical tube. Locally produced drinking water was used for the experiments.

For this research, we examined calcite pellets (100% $CaCO_3$) applied in drinking water softening. Polydisperse calcite pellets were dried, sieved and fractionated in order to acquire more uniformly dispersed samples. Photographic material and standard operating procedure are included in the Supplementary Material (Sections 1 and 2).

Table 1
Parameters and settings used in simulations. Fluid properties are taken at 20 °C; coefficients of friction and restitution are based on the work of Joseph and Hunt (2004).

Variable	Symbol	Value	Unit
Column diameter	D	0.057	[m]
Column length	C	2.0	[m]
CFD cell size	Δx	4.65	[mm]
CFD time step	Δt_{CFD}	10^{-3}	[s]
DEM time step	Δt_{DEM}	10^{-5}	[s]
Fluid density	ρ_f	998.20	[kg/m^3]
Fluid dynamic viscosity	η_f	$1.005{\cdot}10^{-3}$	[Pa·s]
Particle diameter (mean)	$\langle d_p \rangle$	1.55	[mm]
Particle diameter (standard deviation)	σ_p	0.16	[mm]
Particle density	ρ_p	2575	[kg/m^3]
Total particle mass	m_p	0.87	[kg]
Particle Young's modulus	Y_p	5.0	[MPa]
Particle Poisson ratio	ν_p	0.45	[-]
Particle coefficient of restitution	e_p	0.3	[-]
Particle coefficient of friction	μ_p	0.05	[-]

2.3. Camera experiments

In this study, we used a Chronos 1.4 high-speed camera to make video recordings of the collective motion of calcite pellets ($1.4 < d_p < 1.7$ mm) in the expansion column at different flow rates. This camera is capable of capturing images at a rate of 1.4 gigapixel per second (Kramer et al., 2020a). We varied the superficial fluid velocity between 15 and 87 mm/s (corresponding to bed voidages between 0.42 and 0.78) and used recording rates increasing from 10 to 1200 fps, as shown in Table 2. In addition, video recordings were made with a Canon LEGRIA HF G25 (1920 × 1080 pixels at 25 fps) for various flow rates. Besides the ($1.4 < d_p < 1.7$ mm) pellets, ($0.8 < d_p < 0.9$ mm) pellets were also recorded (Kramer et al., 2020d).

3. Results and discussion

3.1. Expansion experiments

Fluidisation characteristics were measured for calcite pellets ($1.4 < d_p < 1.7$ mm, ρ_p = 2,575 kg/m^3) at 20 °C for five different superficial fluid velocities. Some experiments were executed in *duplo* or *triplo*, as shown in Table 2. Additionally, videos were made for two types of calcite pellets: Geldart's type D ($1.4 < d_p < 1.7$ mm) and Geldart's type B ($0.8 < d_p < 0.9$ mm) (Geldart, 1973). For validation purposes, additional expansion characteristics were acquired for varying temperatures and flow rates. The experimental data is included in full in the Supplementary Material (Section 7).

3.2. Fluidisation characterisation observations

During the fluidisation experiments with calcite grains, open spaces and voids of water were observed between the fluidised particles (Fig. 4), even at relatively low fluid velocities in the vicinity of minimum fluidisation. These voids were found to increase in size when the fluid flow increased (Kramer et al., 2020c).

Voids are formed when the pathway between clusters of particles is of lesser resistance than the assumed homogeneous fluidisation state, resulting in a lower energy dissipation. A liquid–solid fluidised bed may appear homogeneous when observed on a larger scale, but locally the fluid flow distribution through the bed may notbe completely uniform. These inhomogeneities appear in the form of bubbles, travelling waves or particle clusters (parvoids) depending on the systems physical parameters (Hassett, 1961).

Moreover, significant heterogeneous particle–fluid patterns were detected at higher fluid velocities. The observed voids behaved like bubbly waves (Verloop and Heertjes, 1970) and moved up the bed with a certain wave velocity and frequency. Around these voids, clusters of particles were formed, which had a tendency to linger as a group and show decreased hindered settling. After individual particles broke loose from the particle train and start settling vertically, the remaining particles followed successively. For relatively high fluid velocities, recirculation patterns were observed where particles tended to show both upward and downward flow. At these high fluid velocities, the voids were more equidistantly distributed in the bed. In the vicinity of the column walls, the bed voidage was slightly higher compared to the bulk of the fluidised bed, which consequently implies a slightly different hydrodynamic flow pattern, as confirmed by (Loeffler, 1953). According to the transition model for LSF by Gibilaro et al. (1986), the considered 1.4–1.7 mm calcite pellets should belong to the fully particulate (homogeneous) region, not to the aggregate region nor to the particulate and aggregate regions. In contrast to the transition model, a homogeneous state for these examined particles was not observed in experiments.

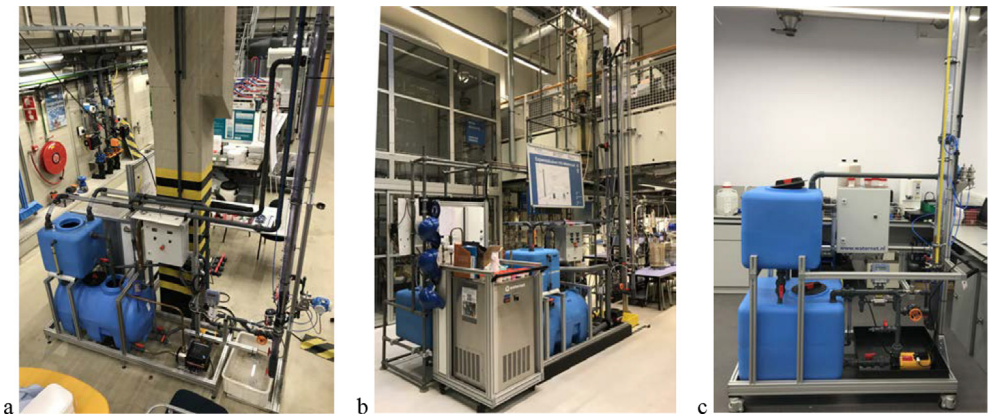

Fig. 2. Photographs of the expansion columns located at Waternet (a), University of Applied Sciences Utrecht (b) and Queen Mary University of London (c). Additional information about the set-ups and operating procedure is provided in the Supplementary Material (Section 2).

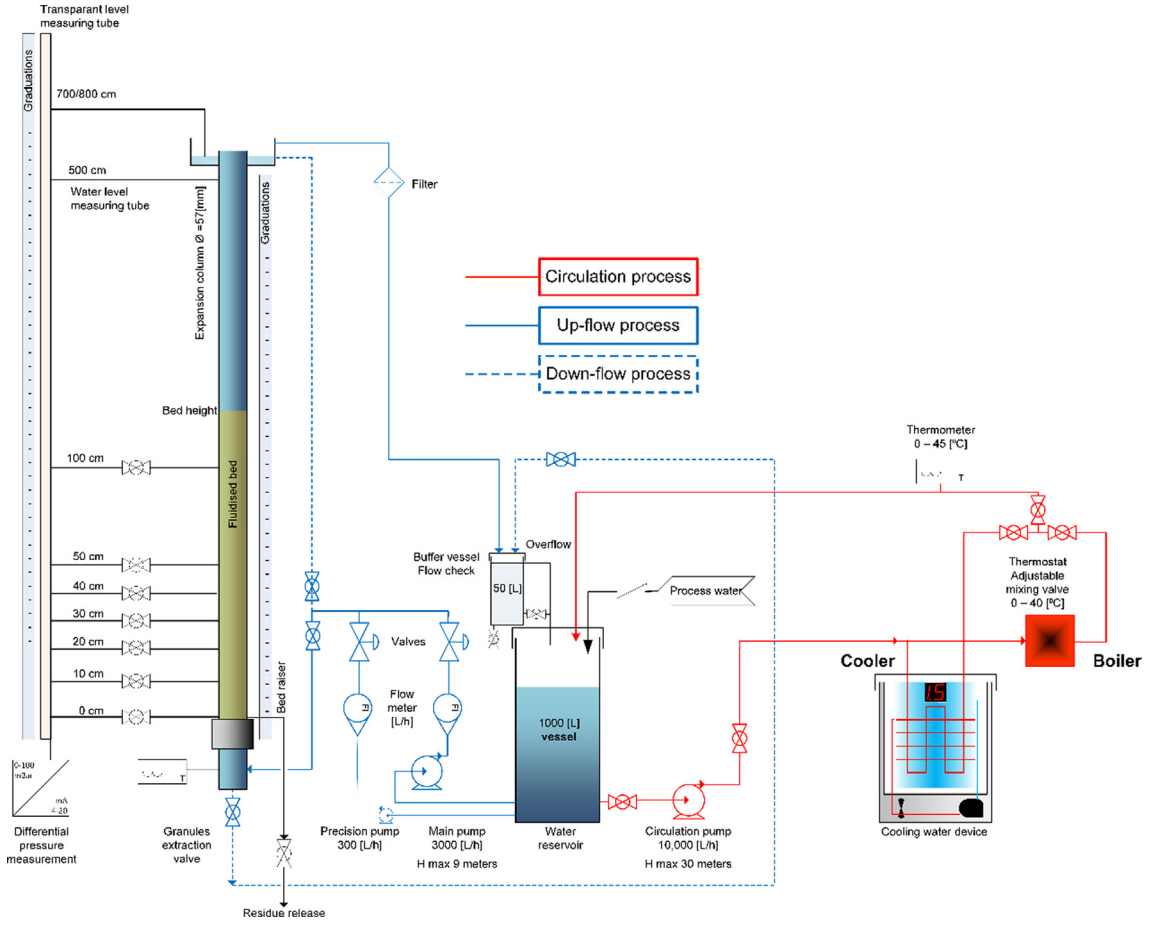

Fig. 3. Schematic representation of the experimental set-up, showing the cylindrical column, the main expansion circuit (blue) and the temperature conditioning circuit (red). (For interpretation of the references to colour in this figure legend, the reader is referred to the web version of this article.)

Table 2
Experimental and numerical results for 1.4–1.7 mm calcite pellets in water at 20 °C.

Nr. [#]	Superficial fluid velocity [mm/s]	Ratio superficial to terminal selling velocity [-]	Bed voidage numerical [-]	Bed voidage experimental [-]	Pressure drop numerical [kPa]	Pressure drop experimental [kPa]	Frame rate [fps]
1,2,3	15	0.015	0.38	0.42	2.06	2.08	10
4,5	30	0.030	0.48	0.54	2.07	2.08	10
6,7,8	61	0.061	0.59	0.68	2.10	2.08	400
9	87	0.087	0.70	0.78	2.15	2.08	600
10	142	0.142	0.89	0.91	2.16	2.08	1200

Fig. 4. Sequence of 1.4–1.7 mm calcite pellets in a 57 mm column. Dark zones are caused by local pockets of water, v_s= 25 mm/s, $\langle\varepsilon\rangle$ = 0.50, average interstitial fluid velocity 50 mm/s. White lines represent the progression of waves of voids moving up at 50 mm/s. The time interval between images is 0.17 s, corresponding to 8.5 mm or 5.5 particle diameters. The wave progression can be seen more clearly on the provided video material (Kramer, 2020); (Kramer et al., 2020a); (Kramer et al., 2020d).

3.3. Simulation results and discussion

The mean bed voidage for calcite pellets fraction 1.4 < d_p [mm] < 1.7 was predicted on the basis of the CFD-DEM simulations carried out by Nijssen et al. (2020) and compared with the experimentally determined voidages (Kramer et al., 2020c). In addition, the voidages were estimated with the popular model developed by Richardson and Zaki (1954) and an empirical model proposed by Kramer et al. (2020b).

The results presented in Fig. 5 show that the CFD-DEM model under-predicts the voidage by a relative error of up to 10%, especially at intermediate flow rates. The voidage prediction for the Richardson-Zaki model has the largest discrepancy compared to the experimentally measured values, while the empirical model proposed by Kramer *et al.* shows the smallest deviation. The latter may not come as a surprise, since this data-driven model was calibrated for a variety of calcite pellet fractions.

Table 2 shows the basic bed characteristics obtained from the CFD-DEM simulations. The authors believe that the discrepancy with the experimental values in Table 2 is mainly caused by the non-spherical shape of the particles (Dharmarajah, 1982). Photographs of the calcite pellets are included in the Supplementary Material (Section 1). Analysis of these images has indicated that the particle sphericity can be as low as 0.75. This aspect was not accounted for in the simulations. Nevertheless, the trend of the expansion is captured accurately, and analysis of the simulation results yields valuable insight into the bed behaviour.

Fig. 6 shows an instantaneous CFD-DEM snapshot of the bed voidage in a cross-section through the centre of the bed, and

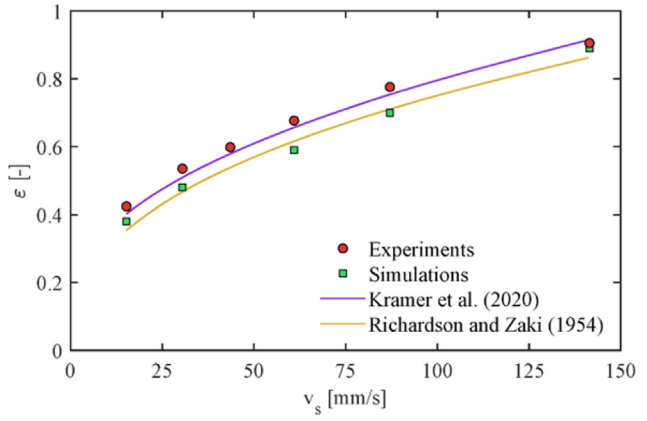

Fig. 5. Experimentally measured mean voidage (circles), mean voidage predicted by CFD-DEM simulations (squares) (Nijssen et al., 2020) (ARE = 10%), empirical data-driven model (purple line) (Kramer et al., 2020b) (ARE = 2%), and a popular model (amber line) (Richardson and Zaki, 1954) (ARE = 15%) for calcite pellets range 1.4 < d_p [mm] < 1.7. (For interpretation of the references to colour in this figure legend, the reader is referred to the web version of this article.)

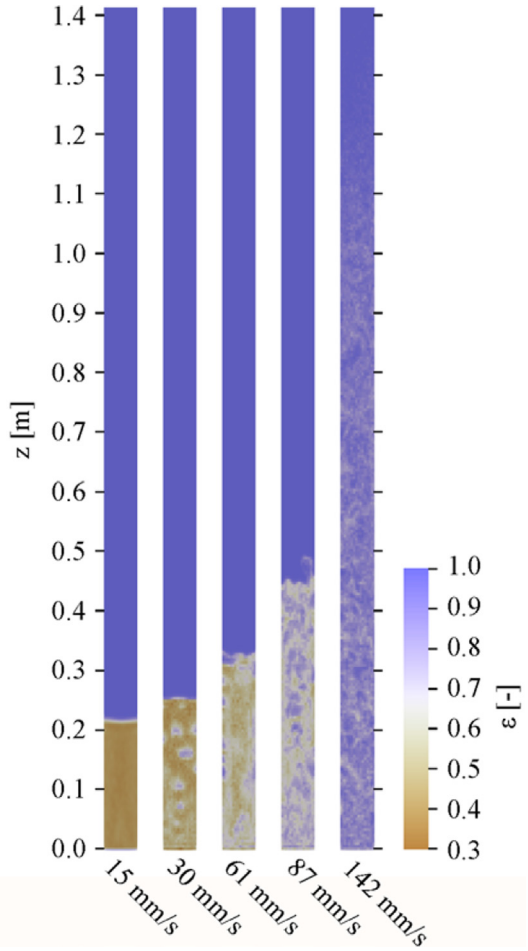

Fig. 6. Instantaneous cross-sectional voidage snapshots for increasing superficial liquid velocity (15, 30, 61, 87 and 142 mm/s, respectively). Videos of the simulation can be assessed at: (Kramer and Nijssen, 2021).

Fig. 7 shows the particle distribution (particles coloured by size) as viewed from the outside. The bed appears to be homogeneous when the particles are observed from outside the bed (Fig. 7). However, Fig. 6 shows the appearance of discrete water pockets at lower superficial liquid velocity, which transform into more complex structures at higher velocities. At the highest flow rate, the bed is composed of thin, interwoven particle-dense and dilute regions. Furthermore, it can be seen that only at high fluid velocity stratification of the bed is obtained. This indicates mobility of the particles but an absence of a large-scale mixing pattern. Separation of the smallest particles is observed at the lowest velocity, but stratification of the entire bed is not found.

The time-averaged solid mass flux was obtained from each simulation and is shown in Fig. 8. This figure shows the vertical flux through a horizontal plane at height $z = L/2$. A weak overall solids circulation exists at intermediate velocity, which was also observed in the experiments. Depending on the superficial fluid velocity, upward particle movement can occur through the bed centre or along the walls. This indicates that the circulation pattern is rather unstable and might be highly susceptible to changes in the initial bed configuration or the liquid distribution. The unstable circulation is confirmed by standard deviations reported in Table 3, which were calculated at the centre of the bed. Above the lowest fluid velocity, the standard deviation is of the same order as the mean solid mass flux, indicating a widely varying solids movement.

The strongest circulation can be found at v_s = 30 mm/s, corresponding to water pockets moving up through the centre of the bed, as observed in Fig. 6. At the highest liquid velocity, approaching the particle terminal settling velocity (200 < v_t [mm/s] ⟨2 3 5), the time-averaged solids circulation vanishes. As can be seen from the standard deviation in Table 3, the fluctuating component persists. This lack of large-scale solids mixing combined with particle mobility allows for the stratification at high velocity as represented in Fig. 7.

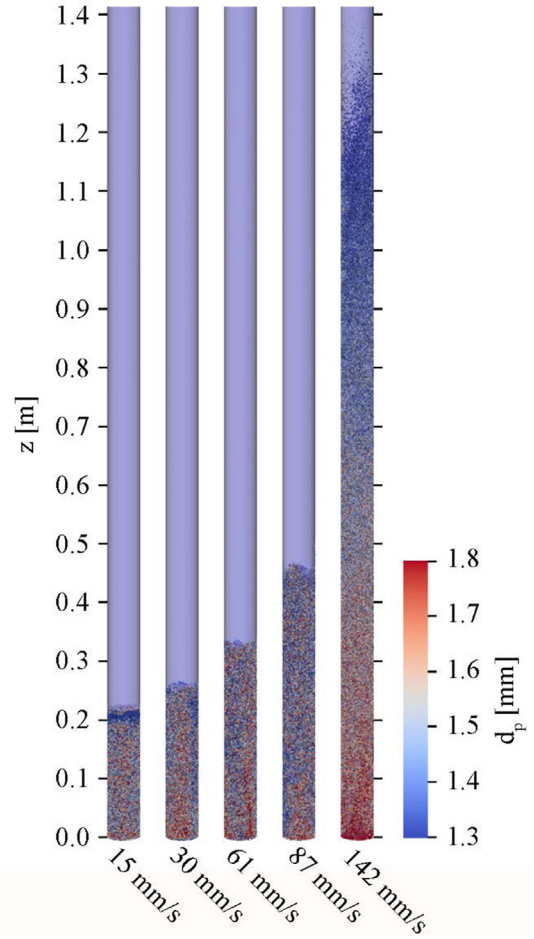

Fig. 7. Instantaneous snapshots of particle distribution for increasing superficial liquid velocity (15, 30, 61, 87 and 142 mm/s, respectively). Colours indicate particle size.

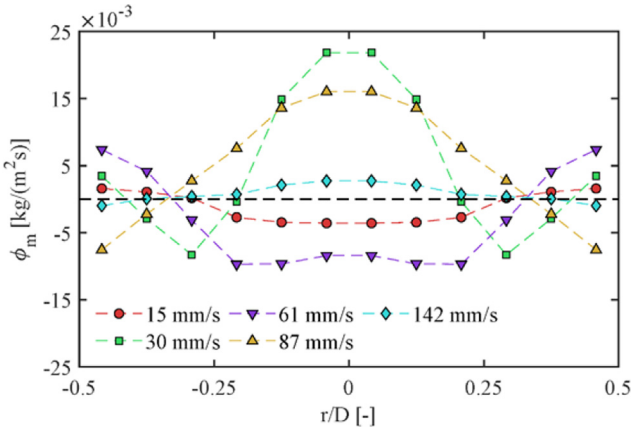

Fig. 8. Time-averaged vertical solid mass flux at different superficial liquid velocity, measured at z = $L/2$.

Table 3
Time-averaged vertical mass flux at the bed centre and corresponding standard deviation, measured at z = $L/2$.

Superficial fluid velocity [mm/s]	Mean solid mass flux [10^{-3} kg/(m^{2}s)]	Solid mass flux standard deviation [10^{-3} kg/(m^{2}s)]
15	−3.56	0.23
30	21.9	12.6
61	−8.42	25.3
87	16.0	16.2
142	2.72	4.89

A visual comparison of void development in experiments and simulations with increasing fluid velocity is shown in Fig. 9. At v_s =30 mm/s (Fig. 9c and d) the simulations predict large singular voids, while experiments show more numerous smaller pockets of water. At higher fluid flows, the particle structure opens up further and voids merge into larger structures. This was captured both in experiments and in simulations. As the fluid motion is not resolved at the particle scale in the CFD-DEM method, prediction of the actual void shape is precarious. Still, a qualitative comparison of void size holds very well, especially at higher liquid velocities.

To further quantify the influence of the observed voids on the operational efficiency of the LSF bed reactor, the probability density function (PDF, (Eq. (1)) of the local voidage and its derived cumulative distribution function (CDF, Eq. (2)) were evaluated. In the equations below, $V(\varepsilon)d\varepsilon$ denotes the total volume of cells having void fraction between ε and $\varepsilon + d\varepsilon$. Furthermore, a distinction has been made between the layer of cells bordering the reactor wall and those in the core of the reactor.

$$PDF(\varepsilon)d\varepsilon = \frac{V(\varepsilon)d\varepsilon}{\int_0^1 V(\varepsilon)d\widehat{\varepsilon}} \tag{1}$$

$$CDF(\varepsilon) = \int_0^{\varepsilon} PDF(\widehat{\varepsilon})d\widehat{\varepsilon} \tag{2}$$

$$\langle\varepsilon\rangle = \int_0^1 PDF(\widehat{\varepsilon}) \cdot \widehat{\varepsilon}d\widehat{\varepsilon} \tag{3}$$

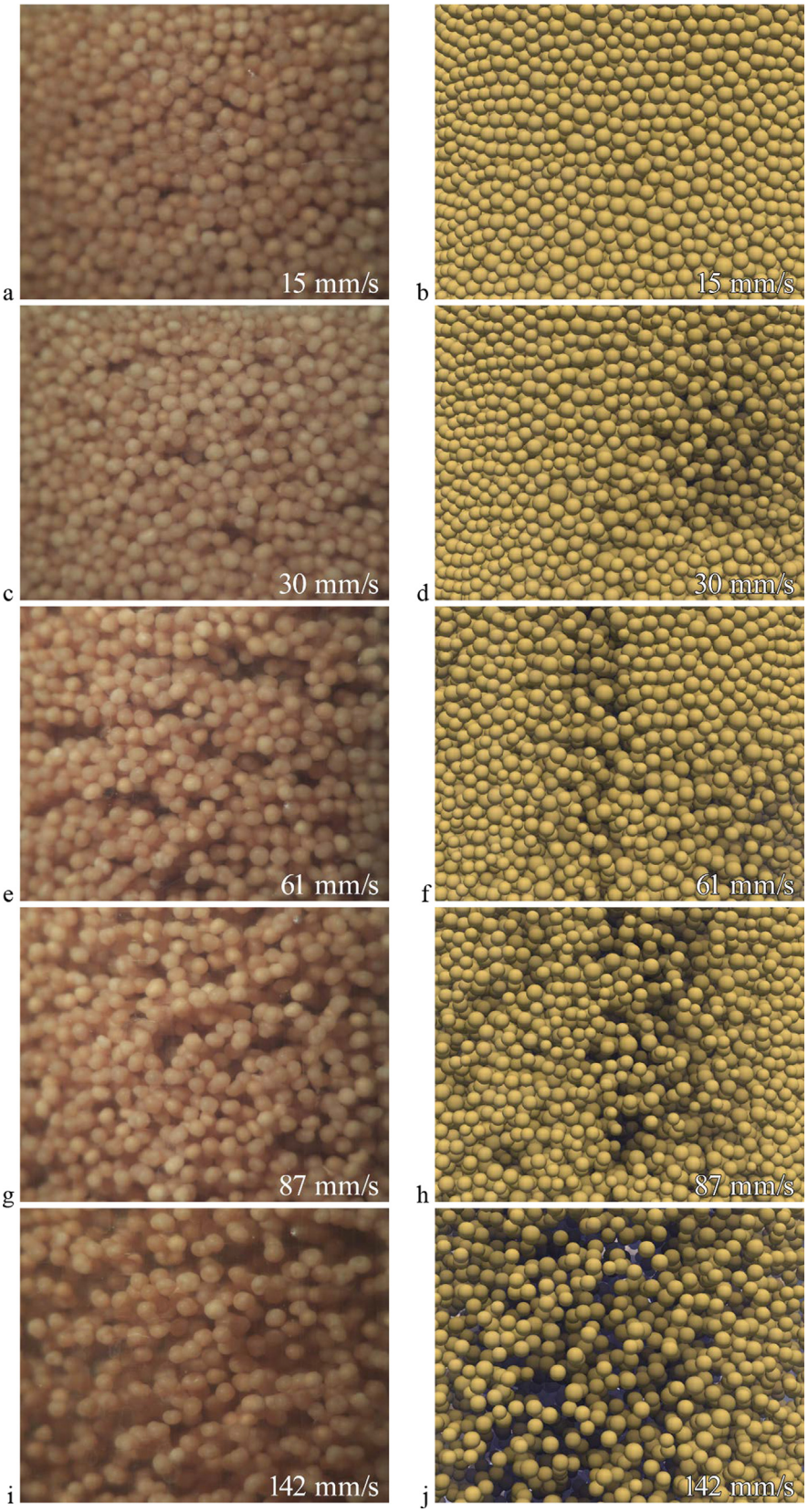

Fig. 9. Visual comparison between experiments (left) and simulations (right), showing void development with increasing superficial liquid velocity (15, 30, 61, 87 and 142 mm/s, respectively).

$$\sigma_{\varepsilon}^2 = \int_0^1 PDF(\widehat{\varepsilon}) \cdot (\widehat{\varepsilon} - \langle\varepsilon\rangle)^2 d\widehat{\varepsilon} \quad (4)$$

By way of illustration, Fig. 10 shows the voidage PDF for the simulation with v_s = 30 mm/s. The results obtained at other fluid velocities are included in the Supplementary Material (Section 4). The dashed lines indicate the mean voidage (Eq. (3)) in the wall and core regions, while the dotted lines indicate the range of voidage encompassing 95% of the bed volume ($CDF(\varepsilon)$ = 2.5% and 97.5%). Clearly, the void fraction distribution is not symmetrical, showing a peak at low voidage with a long tail reaching up to 90% liquid volume. This indicates the presence of high-voidage water bubbles in a denser emulsion phase. The broad distribution means that the mean bed voidage is not an adequate parameter to describe the LSF bed state, as a range of voidages should be considered instead.

Lastly, the voidage in the vicinity of the reactor walls was found to be up to 5% higher than in the bulk of the bed. This indicates an intrinsic limitation of optical voidage measurements in LSF bed experiments. The liquid volume fraction measured close to the wall is not representative of that in the core of the reactor. Simulations offer an advantage, as they provide full 3D void fraction information without the need for expensive measurement techniques, such as x-ray tomography, electrical capacitance tomography or optical probing.

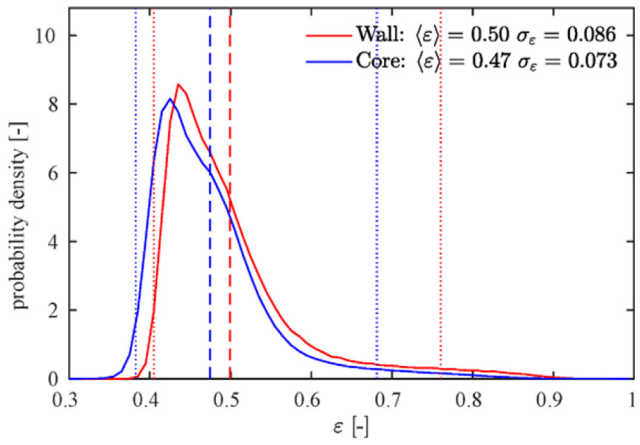

Fig. 10. Voidage probability density function obtained at v_s = 30 mm/s. Dashed lines indicate mean voidage; dotted lines mark the range of voidages comprising 95% of the bed volume.

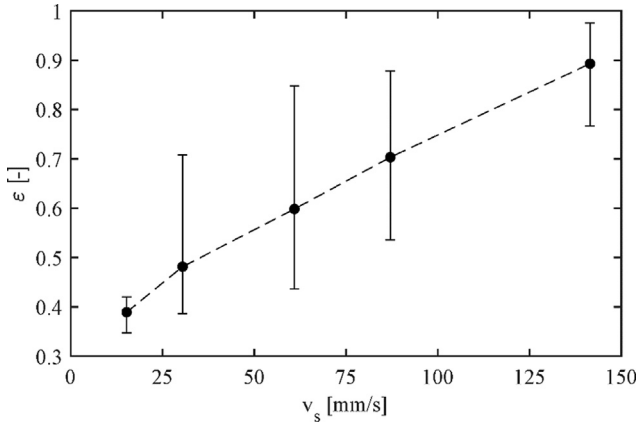

Fig. 11. LSF bed expansion behaviour with increasing superficial liquid velocity. Symbols indicate mean voidage, error bars signify the range of voidages comprising 95% of the bed volume. Minimum fluidisation velocities: v_{mf} = 13.6 mm/s for d_p = 1.4 mm and v_{mf} = 17.2 mm/s for d_p = 1.7 mm calcite pellets.

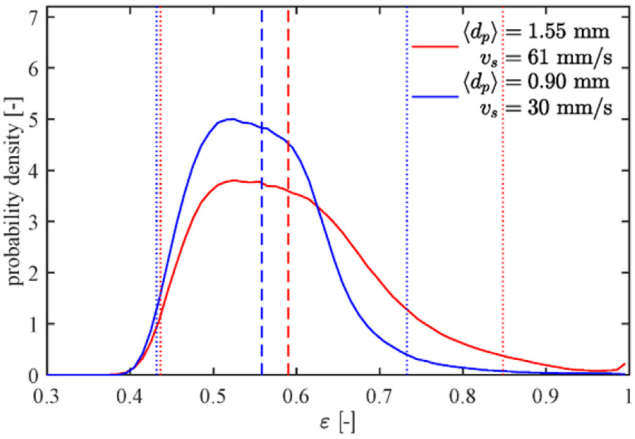

Fig. 12. Comparison of voidage probability density functions for large particles ($\langle d_p \rangle$ = 1.55 mm, σ_p = 0.16 mm, v_s = 61 mm/s) and small particles ($\langle d_p \rangle$ = 0.9 mm, σ_p = 0.08 mm, v_s = 30 mm/s) at similar mean voidage. Dashed lines indicate mean voidage; dotted lines mark the range of voidages comprising 95% of the bed volume.

The heterogeneity of the bed observed in the simulations is summarised in Fig. 11. Symbols show the mean voidage plotted against superficial fluid velocity, while the error bars indicate the range of voidages comprising 95% of the bed volume. Interestingly, heterogeneity shows to be most pronounced slightly above the onset of fluidisation (Fig. 11). At higher velocity, the range of observed voidages narrows as the discrete bubbles transform into more complex structures.

In order to show the influence of particle size on the bed heterogeneity, a simulation was repeated using smaller particles $\langle d_p \rangle$ = 0.9 mm, σ_p = 0.08 mm, v_s = 30 mm/s. The obtained voidage PDF is shown in Fig. 12 and compared with previous results at v_s = 61 mm/s. These two simulations are compared in view of their similar expansion, *i.e.* mean voidage. However, the range of observed voidages is much narrower using smaller particles. This clearly indicates that larger particles favour a more heterogeneous bed configuration, as was previously shown by Di Felice (1995). In addition to being narrower, the distribution obtained from smaller particles is also more symmetric than the distribution found for the larger particles, indicating a less distinct separation between the emulsion and bubble phases.

4. Conclusions

In this work, both experiments and simulations were employed to gain insight into the heterogeneous behaviour of drinking water softening reactors. In the literature, LSF systems are often considered to be homogeneous at modest velocities. Nevertheless, in the experiments with calcite grains, local voids were observed at relatively low fluid velocities and significant heterogeneous particle–fluid patterns at higher fluid velocities. A CFD-DEM simulation model was used, and its results compared with expansion measurements and high-speed videos and images. From this combination of experiments and simulations, it was concluded that homogeneous fluidisation virtually does not occur.

In the literature, fluidisation behaviour is usually investigated either through experimental work or numerical modelling. Considering their respective advantages and disadvantages, the combination of a numerical model and experiments proved to be a highly effective way to investigate this complex system. Experiments were needed to measure bed expansion, *i.e.* mean voidage, and to observe fluidisation features and patterns from the outside of the reactor (quasi 2D). The simulations made it possible to explore the fluidisation features and patterns even further, allowing mea-

surements throughout the entire bed (3D). This has yielded important new insights into LSF behaviour.

The heterogeneity and onset of fluidisation behaviour obtained from the simulations and experimental observations were compared and found to agree reasonably well. The simulations showed distinct differences in void fraction in the cross-section of the columns. The voidage in the vicinity of the wall was not representative of that in the core of the reactor. Furthermore, the voidage distribution in the fluidised bed was found to be broadest at intermediate velocity. This information is of paramount importance for the chemical performance of the water softening reactor. Lastly, the solids circulation was investigated by measuring the solids flux. The circulation pattern was found to be unstable and prone to inversion. As expected, the solids flux vanished as the liquid velocity approached the particle terminal velocity.

5. Recommendations

It has been shown that CFD-DEM simulations are an effective and reliable tool for the analysis of LSF bed reactors. Using this method, much can be learned about liquid–solid fluidisation behaviour. The influence of particle shape and size distribution, liquid properties, as well as reactor scale are all subjects of major interest to which this method can be applied. The accuracy of the method can be improved further through the application of a sphericity correction to the interaction forces, as was discussed by Mema and Padding (2021). Unfortunately, such a correction is not yet available for the unsteady interaction forces. Additionally, a more elaborate model for the kinetic energy dissipation during immersed collisions and influence of lubrication forces will greatly benefit the accuracy of the method.

In this research, unsteady behaviour was observed in LSF bed. It is recommended to conduct future research to better define and quantify the degree of heterogeneity, *i.e.* improve the fluidisation quality definitions and terms related to the fluid and particle properties.

We have enabled future numerical and experimental studies to investigate the impact of these properties on reactor performance in full-scale treatment processes such as pellet softening. Since it remains unclear whether heterogeneous behaviour could be beneficial or disadvantageous for chemical crystallisation efficiency in full-scale pellet-softening reactors, the CFD-DEM method could be used in future research with the aim to discover optimisation solutions. To this end, species transfer equations and chemical reactors can be added to the model to capture the influence of hydrodynamics and the chemical performance of the reactor.

CRediT authorship contribution statement

T.M.J. Nijssen: Conceptualization, Methodology, Software, Validation, Formal analysis, Investigation, Data curation, Writing - original draft, Visualization. **O.J.I. Kramer:** Conceptualization, Methodology, Validation, Formal analysis, Investigation, Data curation, Writing - original draft, Visualization. **P.J. de Moel:** Conceptualization, Visualization, Methodology, Validation. **J. Rahman:** Methodology, Validation, Formal analysis, Writing - original draft, Visualization. **J.P. Kroon:** Methodology, Software, Validation, Formal analysis. **P. Berhanu:** Methodology, Validation, Writing - original draft, Investigation. **E.S. Boek:** Conceptualization, Writing - review & editing. **K.A. Buist:** Conceptualization, Writing - review & editing, Supervision, Project administration, Funding acquisition. **J.P. van der Hoek:** Writing - review & editing, Supervision, Project administration, Funding acquisition. **J.T. Padding:** Conceptualization, Writing - review & editing, Supervision, Project administration, Funding acquisition. **J.A.M. Kuipers:** Conceptualization, Writing - review & editing, Supervision, Project administration, Funding acquisition.

Declaration of Competing Interest

The authors declare that they have no known competing financial interests or personal relationships that could have appeared to influence the work reported in this paper.

Acknowledgements

We acknowledge and thank our students from Delft University of Technology, Eindhoven University of Technology, HU University of Applied Sciences Utrecht and Queen Mary University of London for the precise execution of many laboratory and pilot plant experiments and simulations. We are grateful to Dr. R. Castrejon-Pita (QMUL) for making his Chronos 1.4 high-speed camera available for our video recordings of calcite pellets at different flow rates.

This research is part of the project "Hydraulic modelling of liquid-solid fluidisation in drinking water treatment processes" carried out by Waternet, Delft University of Technology, and HU University of Applied Sciences Utrecht. Financial support came from Waternet Drinking Water Production Department.

Part of this research was carried out under project number S16046 in the framework of the Partnership Program of the Materials Innovation Institute M2i (www.m2i.nl) and the Technology Foundation STW (www.stw.nl), which is part of the Netherlands Organisation for Scientific Research (www.nwo.nl).

Simulations in this work were carried out using the CFDEMcoupling framework, relying on LIGGGHTS and OpenFOAM.

Appendix A. Supplementary material

Supplementary data to this article can be found online at https://doi.org/10.1016/j.cesx.2021.100100.

References

Albright, J., 2009. Albright's chemical engineering handbook. CRC Press, New-York.
Batchelor, G.K., 1988. A new theory of the instability of a uniform fluidized bed. J. Fluid Mech. 193, 75–110. https://doi.org/10.1017/S002211208800206X.
Beeftink, M., Hofs, B., Kramer, O.J.I., Odegard, I., van der Wal, A., 2021. Carbon footprint of drinking water softening as determined by life cycle assessment. J. Cleaner Prod. 278, 1–10. https://doi.org/10.1016/j.jclepro.2020.123925.
Blais, B., Bertrand, F., 2017. CFD-DEM investigation of viscous solid–liquid mixing: Impact of particle properties and mixer characteristics. Chem. Eng. Res. Des. 118, 270–285. https://doi.org/10.1016/j.cherd.2016.12.018.
Burhenne, L., Giacomin, C., Follett, T., Ritchie, J., McCahill, J.S.J., Mérida, W., 2017. Characterization of reactive CaCO3 crystallization in a fluidized bed reactor as a central process of direct air capture. J. Environ. Chem. Eng. 5, 5968–5977. https://doi.org/10.1016/j.jece.2017.10.047.
Crittenden, J.C., Trussell, R.R., Hand, D.W., Howe, K.J., Tchobanoglous, G., 2012. MWH's water treatment: principles and design. John Wiley & Sons, New York.
Crowe, C.T., Group, F., 2006. Multiphase flow handbook, first ed. Hemisphere. CRC Press, New York.
Davidson, J.F., Clift, R., Harrison, D., 1985. Fluidization. Academic Press Inc, London.
Dharmarajah, A.H., 1982. Effect of particle shape on prediction of velocity-voidage relationship in fluidized solid-liquid systems. Ames.
di Felice, R., 1995. Review article number 47: Of hydrodynamics of liquid fluidisation. Chem. Eng. Sci. 50, 1213–1245. https://doi.org/10.1016/0009-2509(95)98838-6.
Fazle Hussain, A.K., 1986. Coherent structures and turbulence. J. Fluid Mech. 173, 303–356. https://doi.org/10.1017/S0022112086001192.
Geldart, D., 1973. Types of gas fluidization. Powder Technol. 7, 285–292. https://doi.org/10.1016/0032-5910(73)80037-3.
Ghatage, S.v., Peng, Z., Sathe, M.J., Doroodchi, E., Padhiyar, N., Moghtaderi, B., Joshi, J. B., Evans, G.M., 2014. Stability analysis in solid-liquid fluidized beds: experimental and computational. Chem. Eng. J. 256, 169–186. https://doi.org/10.1016/j.cej.2014.06.026.
Gibilaro, L.G., 2001. Fluidization-dynamics, the formulation and applications of a predictive theory for the fluidized state. Butterworth-Heinemann, Oxford.
Gibilaro, L.G., Hossain, I., Foscolo, P.U., 1986. Aggregate behaviour of liquid fluidised beds. Can. J. Chem. Eng. 64, 931–938. https://doi.org/10.1002/cjce.5450640607.

Goossens, W.R.A., 1998. Classification of fluidized particles by Archimedes number. Powder Technol. 98, 48–53. https://doi.org/10.1016/S0032-5910(98)00027-8.
Grace, J.R., Bi, X., Ellis, N., 2020. Essentials of fluidization technology. Wiley-VCH, Vancouver.
Graveland, A.J., van Dijk, J.C., de Moel, P.J., Oomen, J.H.C.M., 1983. Developments in water softening by means of pellet reactors. J. AWWA – Am. Water Works Assoc. 75, 619–625.
Hassett, N.J., 1961. The mechanics of fluidization. British Chem. Eng. 19, 777–780.
Hofman, J.A.M.H., Kramer, O.J.I., van der Hoek, J.P., Nederlof, M.M., Groenendijk, M., 2007. Twenty years of experience with central softening in the Netherlands, water quality, environmental benefits and costs, in: Water 21. In: International Symposium on Health Aspects of Calcium and Magnesium in Drinking Water, MD. International Life Sciences Institute, 24–26 April 2006. Washington, DC., USA, pp. 1–8.
Hu, R.Z., Huang, T.L., Wen, G., Yang, S.Y., 2017. Modelling particle growth of calcium carbonate in a pilot-scale pellet fluidized bed reactor. Water Sci. Technol. Water Supply 17, 643–651. https://doi.org/10.2166/ws.2016.158.
Jamialahmadi, M., Miiller-Steinhagen, H., 1992. Bed voidage in annular solid-liquid fluidized beds. Chem. Eng. Process.
Joseph, G.G., Hunt, M.L., 2004. Oblique particle-wall collisions in a liquid. J. Fluid Mech. 71–93. https://doi.org/10.1017/S002211200400919X.
Kramer, O.J.I., 2020. Videos of liquid-solid fluidisation experiments of calcite pellets and glass beads in water 4TU.Centre for Research Data. 4TU. Centre for Research Data, The Netherlands. https://doi.org/10.4121/uuid:1b685d9e-4441-4a53-865c-86622ba49b25.
Kramer, O.J.I., Castrejon-Pita, J.R., Boek, E.S., 2020. Videos (high speed camera) - liquid-solid fluidisation experiments (calcite-pellets 1.4-1.7 mm in water) [Data set] 4TU.Centre for Research Data. 4TU.Centre for Research Data, Amsterdam, The Netherlands. https://doi.org/10.4121/uuid:41556e6c-b599-42cd-9f1d-bcf01dbe8576.
Kramer, O.J.I., de Moel, P.J., Padding, J.T., Baars, E.T., el Hasadi, Y.M.F., Boek, E.S., van der Hoek, J.P., 2020b. Accurate voidage prediction in fluidisation systems for full-scale drinking water pellet softening reactors using data driven models. J. Water Process Eng. 37, 1–15. https://doi.org/10.1016/j.jwpe.2020.101481.
Kramer, O.J.I., Nijssen, T.M.J., 2021. Videos – CFD-DEM simulations: fluidisation of calcite-pellets in water 4TU.Centre for Research Data. 4TU.Centre for Research Data, The Netherlands. https://doi.org/10.4121/13663619.
Kramer, O.J.I., Padding, J.T., van Vugt, W.H., de Moel, P.J., Baars, E.T., Boek, E.S., van der Hoek, J.P., 2020c. Improvement of voidage prediction in liquid-solid fluidized beds by inclusion of the Froude number in effective drag relations. Int. J. Multiph. Flow 127. https://doi.org/10.1016/j.ijmultiphaseflow.2020.103261.
Kramer, O.J.I., van Schaik, C., Nijssen, T.M.J., 2020. Videos of fluidisation of calcite-pellets 0.8-0.9mm and 1.4-1.7 mm in water for various flow rates [Data set] 4TU.Centre for Research Data. 4TU.ResearchData, The Netherlands. https://doi.org/10.4121/13277246.v1.
Liu, D., Kwauk, M., Li, H., 1996. Aggregative and particulate fluidization the two extremes of a continuous spectrum. Chem. Eng. Sci. 51 (17), 4045–4063. https://doi.org/https://doi.org/10.1016/0009-2509(96)00247-3.
Liu, G., Wang, P., Wang, S., Sun, L., Yang, Y., Xu, P., 2013. Numerical simulation of flow behavior of liquid and particles in liquid-solid risers with multi scale interfacial drag method. Adv. Powder Technol. 24, 537–548. https://doi.org/10.1016/j.apt.2012.10.007.
Loeffler, A.L., 1953. Mechanism of hindered settling and fluidization. Ames. https://doi.org/10.31274/rtd-180813-14679.
Mema, I., Padding, J.T., 2021. Fluidization of elongated particles - Effect of multi-particle correlations for drag, lift, and torque in CFD-DEM. AIChE J. 1–11. https://doi.org/10.1002/aic.17157.
Michaelide, E., Crowe, C.T., Schwarzkopf, J.D., 2017. Multiphase flow handbook. Taylor & Francis Inc, London.
Nijssen, T.M.J., Kuipers, J.A.M., van der Stel, J., Adema, A.T., Buist, K.A., 2020. Complete liquid-solid momentum coupling for unresolved CFD-DEM simulations. Int. J. Multiph. Flow 132. https://doi.org/10.1016/j.ijmultiphaseflow.2020.103425.
Oke, O., Lettieri, P., Mazzei, L., 2015. An investigation on the mechanics of homogeneous expansion in gas-fluidized beds. Chem. Eng. Sci. 127, 95–105. https://doi.org/10.1016/j.ces.2015.01.020.
Richardson, J.F., Zaki, W.N., 1954. Sedimentation and fluidisation: part I. Trans. Instit. Chem. Eng. 32, 35–53. https://doi.org/10.1016/S0263-8762(97)80006-8.
Rietveld, L.C., 2005. Improving operation of drinking water treatment through modelling.
Ruckenstein, E., 1964. Homogeneous fluidization. Ind. Eng. Chem. Fundam. 3, 260–268. https://doi.org/10.1021/i160011a015.
Schetters, M.J.A., van der Hoek, J.P., Kramer, O.J.I., Kors, L.J., Palmen, L.J., Hofs, B., Koppers, H., 2015. Circular economy in drinking water treatment: re-use of ground pellets as seeding material in the pellet softening process. Water Sci. Technol. 71, 479–486. https://doi.org/10.2166/wst.2014.494.
Tai, C.Y., Chang, M.C., Wu, C.K., Lin, Y.C., 2006. Interpretation of calcite growth data using the two-step crystal growth model. Chem. Eng. Sci. 61, 5346–5354. https://doi.org/10.1016/j.ces.2006.03.047.
Tsuchiya, K., Furumoto, A., Fan, L.S., Zhang, J., 1997. Suspension viscosity and bubble rise velocity in liquid-solid fluidized beds, Chem. Eng. Sci.
van der Veen, C., Graveland, A.J., 1988. Central softening by crystallization in a fluidized-bed process. J. Am. Water Works Assn. 80, 51–58. https://doi.org/10.1002/j.1551-8833.1988.tb03053.x.
van Dijk, J.C., Wilms, D.A., 1991. Water treatment without waste material-fundamentals and state of the art of pellet softening. J. Water Supply: Res. Technol.: AQUA 40, 263–280.
van Schagen, K.M., 2009. Model-based control of drinking-water treatment plants. Delft.
Verloop, J., Heertjes, P.M., 1970. Shock waves as a criterion for the transition from homogeneous to heterogeneous fluidization. Chem. Eng. Sci. 25, 825–832. https://doi.org/10.1016/0009-2509(70)85117-X.
Wang, Z.J., Tang, J., Lu, C.X., 2016. Fluidization characteristics of different sizes of quartz particles in the fluidized bed. Pet. Sci. 13, 584–591. https://doi.org/10.1007/s12182-016-0106-5.
Wilhelm, R.H., Kwauk, M., 1948. Fluidization of solid particles. Chem. Eng. Prog. 44, 201–218.
Yang, W.C., 2003. Handbook of fluidization and fluid-particle systems. Chemical Engineering, first ed. CRC Press, New-York. https://doi.org/10.1016/S1672-2515(07)60126-2.
Zheng, Y., Zhu, J.X., Wen, J., Martin, S.A., Bassi, A., Margaritis, A., 1999. The axial hydrodynamic behavior in a liquid-solid circulating fluidized bed. Can. J. Chem. Eng. 77, 284–290. https://doi.org/10.1002/cjce.5450770213.